The Astrophysical Journal, 680:1112–1119, 2008 June 20

THE STRUCTURAL PROPERTIES AND STAR FORMATION HISTORY OF LEO T FROM DEEP LBT PHOTOMETRY[1]

J. T. A. de Jong,[2] J. Harris,[3] M. G. Coleman,[2] N. F. Martin,[2] E. F. Bell,[2] H.-W. Rix,[2] J. M. Hill,[4] E. D. Skillman,[5] D. J. Sand,[3] E. W. Olszewski,[3] D. Zaritsky,[3] D. Thompson,[4] E. Giallongo,[6] R. Ragazzoni,[7] A. DiPaola,[6] J. Farinato,[7] V. Testa,[6] and J. Bechtold[3]

Received 2007 November 19; accepted 2008 February 26

ABSTRACT

We present deep, wide-field *g* and *r* photometry of the transition-type dwarf galaxy Leo T, obtained with the blue arm of the Large Binocular Telescope. The data confirm the presence of both very young (<1 Gyr) and much older (>5 Gyr) stars. We study the structural properties of the old and young stellar populations by preferentially selecting either population on the basis of their color and magnitude. The young population is significantly more concentrated than the old population, with half-light radii of 104 ± 8 and 148 ± 16 pc, respectively, and their centers are slightly offset. Approximately 10% of the total stellar mass is estimated to be represented by the young stellar population. Comparison of the color-magnitude diagram (CMD) with theoretical isochrones, as well as numerical CMD fitting, suggests that star formation began over 10 Gyr ago and continued in recent times until at least a few hundred Myr ago. The CMD-fitting results are indicative of two distinct star formation bursts, with a quiescent period around 3 Gyr ago, albeit at low significance. The results are consistent with no metallicity evolution and a value of $[\mathrm{Fe/H}] \sim -1.5$ over the entire age of the system. Finally, the data show little, if any, sign of tidal distortion of Leo T.

Subject headings: galaxies: individual (Leo T dSph) — galaxies: stellar content — Local Group

Online material: color figure

1. INTRODUCTION

Leo T clearly stands out from the large number of new dwarf galaxies recently discovered (Willman et al. 2005a, 2005b; Zucker et al. 2006a, 2006b; Belokurov et al. 2006, 2007; Irwin et al. 2007; Walsh et al. 2007) around the Milky Way using Sloan Digital Sky Survey (SDSS; York et al. 2000; Adelman-McCarthy et al. 2007) data. It is by far the most distant, located approximately 420 kpc from the Galaxy, and is probably not bound to it. Furthermore, it is the only one that contains very young (<1 Gyr) stars, apart from an old or intermediate-age population, and has detected H I associated with it (Irwin et al. 2007). In terms of its properties, it seems to be a transitional system, as it combines the round, regular structure of dwarf spheroidal galaxies with the presence of gas and the recent star formation that are common in dwarf irregulars.

The other known so-called transition-type dwarf galaxies, DDO 210, Phoenix, Pisces, Antlia, Pegasus, and Leo A (e.g., Mateo 1998; Grebel 2001), are also isolated Local Group members, but they are much brighter than Leo T. Because of its large distance from the Milky Way, it is unlikely that Leo T has been significantly affected by the tidal forces of the Milky Way, which suggests that its current low luminosity is intrinsic. From the velocity dispersion of 19 red giants, Simon & Geha (2007) infer a dark halo mass of $\sim 10^7\ M_\odot$ and a mass-to-light ratio of $\sim 140\ M_\odot/L_{V,\odot}$ for Leo T. From H I observations, Ryan-Weber et al. (2008) infer a lower limit for the total dynamical mass of $\sim 3 \times 10^6\ M_\odot$ and a mass-to-light ratio of $\gtrsim 56\ M_\odot/L_{V,\odot}$. They also detect two distinct components in the neutral hydrogen, one cold (~500 K) and one warm (~6000 K). It is interesting to see that such a low-luminosity system still contains gas and very young stars at the current epoch.

In this work we present deep photometry of Leo T, obtained with the Large Binocular Telescope. We use these data, the deepest data available on Leo T, to study its stellar populations and structural properties. The outline of this paper is as follows. In § 2 we will first describe the data used in this work. On the basis of its color-magnitude diagram (CMD) morphology, we describe the stellar populations present in Leo T in § 3. The structural properties of Leo T are analyzed in § 4, and in § 5 we use CMD-fitting techniques to constrain its star formation history and metallicity evolution. Finally, our conclusions are presented in § 6.

2. DATA

Deep *g*- and *r*-band photometry was obtained with the blue channel of the Large Binocular Camera (LBC; Ragazzoni et al. 2006; Giallongo et al. 2008) mounted at the prime focus of the Large Binocular Telescope (LBT). Recently commissioned, the LBT consists of two 8.4 m mirrors on a single mount (Hill et al. 2006) and is located on Mount Graham in Arizona. The LBC is a wide-field imager consisting of four 2048 pixel × 4608 pixel chips, providing a field of view of $23' \times 23'$ with a pixel size of $0.23''$. The data, obtained as part of the LBT Science Demonstration Time program, were taken on 2007 March 21 under seeing conditions of $1.0''$–$1.1''$. In each filter, four exposures of 5 minutes

[1] Based on data acquired using the Large Binocular Telescope (LBT). The LBT is an international collaboration among institutions in the United States, Italy, and Germany. The LBT Corporation partners are the University of Arizona, on behalf of the Arizona university system; Istituto Nazionale di Astrofisica, Italy; LBT Beteiligungsgesellschaft, Germany, representing the Max Planck Society, the Astrophysical Institute Potsdam, and Heidelberg University; The Ohio State University; and The Research Corporation, on behalf of the University of Notre Dame, the University of Minnesota, and the University of Virginia.

[2] Max-Planck-Institut für Astronomie, Königstuhl 17, D-69117 Heidelberg, Germany; dejong@mpia.de.

[3] Steward Observatory, University of Arizona, 933 North Cherry Avenue, Tucson, AZ 85721-0065.

[4] Large Binocular Telescope Observatory, University of Arizona, 933 North Cherry Avenue, Tucson, AZ 85721.

[5] Department of Astronomy, University of Minnesota, Minneapolis, MN 55455.

[6] INAF, Osservatorio Astronomico di Roma, via di Frascati 33, I-00040 Monteporzio, Italy.

[7] INAF, Osservatorio Astronomico di Padova, vicolo dell'Osservatorio 5, I-35122 Padova, Italy.

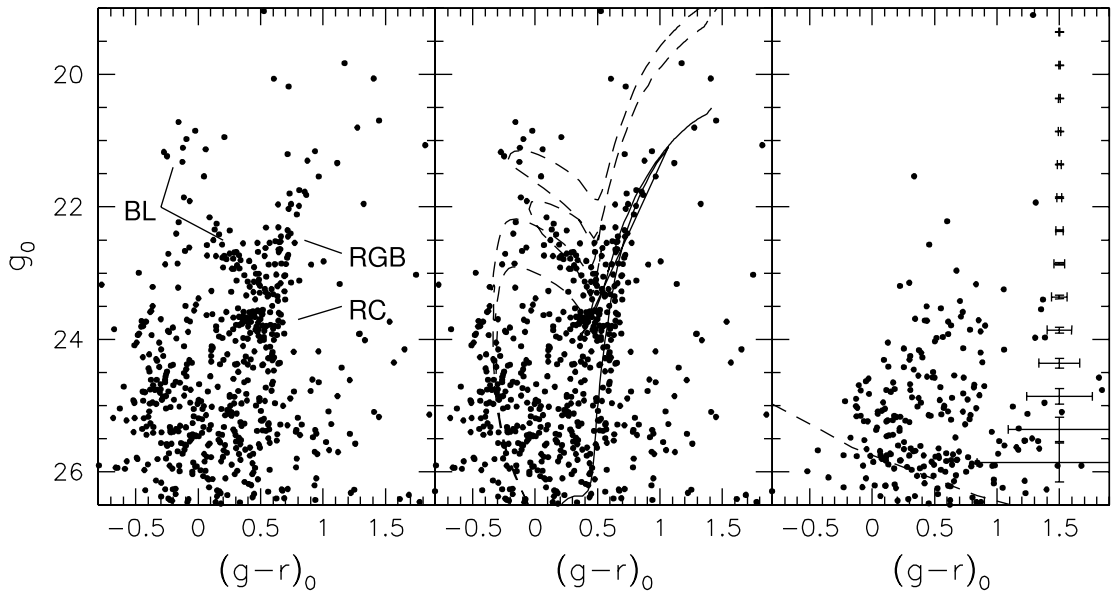

FIG. 1.—*Left*: CMD of stars within 1.4′ of the center of Leo T, with the features discussed in § 3 indicated. *Middle*: Same CMD as at left, but now with isochrones overlaid to outline the two distinct stellar populations. The dashed lines are for 400 and 650 Myr, from left to right; the solid line is for 10 Gyr; and all lines assume that [Fe/H] = −1.7 and $m - M = 23.1$ mag. *Right*: CMD of an annulus of equal area at a radius of 6′ centered on Leo T as the target region, which serves as a control field. Photometric errors are indicated on the right, and the dashed line shows the 50% completeness limit.

each were taken with small offsets to help with bad pixels and cosmic-ray rejection. One *r*-band frame was not used for the current work because of poor guiding.

Data reduction was performed using the reduction pipeline developed by Coleman et al. (2007), which is based on standard routines in the IRAF package `mscred`. The images were trimmed, bias-subtracted, and flat-fielded using the combined twilight flats. Because of the "fast" focal ratio ($f/1.14$) of the LBT primary mirrors, there is significant field distortion (1.75%) near the edges of the field of view. This distortion was removed with a quadratic radial correction to an accuracy of $\sim 0.2''$. Because of the effectively different pixel scale, the photometry must also be flattened before co-adding the single chip images into mosaics. After that, the images were astrometrically registered (with an accuracy of $\sim 0.1''$ with respect to the SDSS catalog) and median-combined to produce the final science frames.

Detection of stars and photometry was performed using the PSF-fitting photometry package DAOPHOT. Because the observations were done in filters that are very close to the SDSS *g* and *r* filters, the photometry was calibrated to the SDSS without the need for standard star observations or atmospheric extinction corrections. The accuracy of the zero-point calibration was $\delta g \sim 0.03$ mag and $\delta r \sim 0.02$ mag. On the basis of the dust extinction maps from Schlegel et al. (1998), the photometry was corrected star by star for foreground extinction; the extinction in the Leo T field varies between $E(B - V) = 0.027$ and 0.041 mag, with a mean of $E(B - V) = 0.035$ mag. For clarity, we will refer to the extinction-corrected magnitudes as g_0 and r_0 in the remainder of this paper. The photometric uncertainties and completeness were determined with artificial star tests. In these tests, 1600 artificial stars were placed at 0.25 mag intervals between the 16th and 29th magnitudes in the *g* and *r* images and were subsequently detected and photometered using DAOPHOT. The photometric uncertainty is taken to be the dispersion of the recovered magnitudes around the mean magnitude.

The resulting color-magnitude diagram (CMD) of the central 1.4′, which is the half-light radius, according to Irwin et al. (2007), of Leo T, is shown in the left and middle panels of Figure 1. In the right panel, the CMD of an annulus of equal area at a radius of 6′ from the center of Leo T is shown; the photometric errors and 50% completeness limit are also indicated in this panel.

3. STELLAR POPULATIONS

Before turning to an analysis of the structure of the Leo T dwarf galaxy, we spend some time describing its two main stellar populations, as previously defined by Irwin et al. (2007). The structural properties of these two populations will then be studied separately.

In the CMD in the left panel of Figure 1, several features are readily visible:

1. a red giant branch (RGB) starting at $(g - r,\ g)_0 \sim (1.3, 21)$ and going all the way down to $\sim$(0.5, 26);
2. a red clump (RC) feature around $(g - r,\ g)_0 \sim (0.4,\ 23.7)$;
3. a ridge of stars between $(g - r,\ g)_0 \sim (0.5,\ 23.3)$ and (0.0, 22.5), reminiscent of a blue loop (BL);
4. a small group of stars around (0.0, 21.0), possibly also related to the BL;
5. an excess of stars bluer than $(g - r)_0 = 0.0$, presumably young main-sequence (MS) stars.

The RGB, RC, and BL were also identified by Irwin et al. (2007), who attributed the first two to an intermediate-age to old population ($\sim$5–12 Gyr) and the latter to a very young (<1 Gyr) population. In Figure 2 we present smoothed, background-subtracted Hess diagrams (two-dimensional histograms of stellar density in the color-magnitude plane; Hess 1924) of our photometry in the central region of Leo T. In § 5 we will redetermine the distance to Leo T, but for the moment we assume the distance modulus of 23.1 mag from the discovery paper (based on horizontal branch [HB] luminosity and CMD fitting) and overlay three isochrones from Girardi et al. (2004) for ages of 5, 8, and 12.5 Gyr and a metallicity of [Fe/H] = −1.7 dex in Figure 2*a*. It is clear that all three isochrones fit the RGB and RC very well and that photometry down to the turnoff ($g \sim 27$ for 12.5 Gyr) will be necessary in order to constrain the age of this older stellar population. In Figure 2*b*, three 8 Gyr isochrones of [Fe/H] = −2.3,

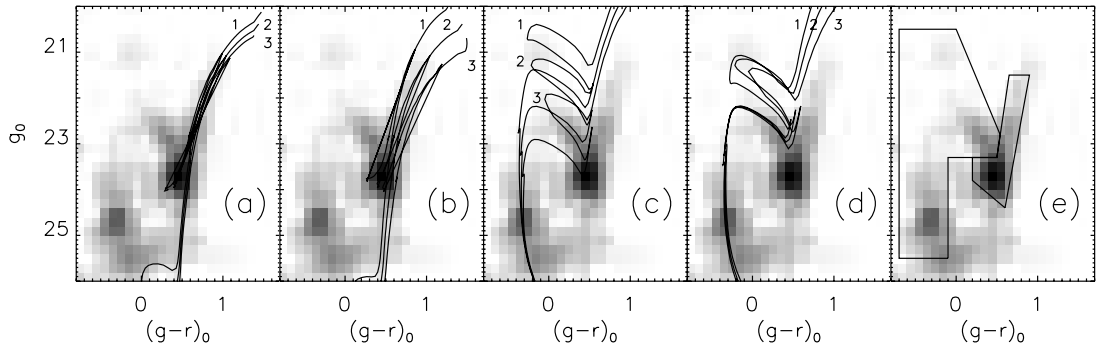

FIG. 2.—Background-subtracted Hess diagrams of Leo T with different overlays: (*a*) isochrones of 5 (line 1), 8 (line 2), and 12.5 Gyr (line 3), with [Fe/H] = −1.7 dex; (*b*) isochrones of 8 Gyr for metallicities of [Fe/H] = −2.3 (line 1), −1.7 (line 2), and −1.3 dex (line 3); (*c*) isochrones of 250 (line 1), 400 (line 2), and 650 (line 3) Myr, with [Fe/H] = −1.7 dex; (*d*) isochrones of 400 Myr for metallicities of [Fe/H] = −2.3 (line 1), −1.7 (line 2), and −1.3 dex (line 3); and (*e*) CMD selection boxes, to select preferentially either stars belonging to the young (*left-hand region*) or the old (*right-hand region*) stellar populations. The Hess diagrams were created by subtracting the scaled Hess diagram of the region outside 6′ from the center of Leo T from that of the region within 1.4′, after which a boxcar smoothing of width 2 is applied.

−1.7, and −1.3 dex are overlaid on the Hess diagram, indicating that both the average color of the RC and the slope of the RGB favor a metallicity of −1.7 dex.

Isochrones for much younger ages of 250, 400, and 650 Myr and [Fe/H] = −1.7 dex are overplotted on the Hess diagram in Figure 2*c*. This clearly implies that the stars blueward of $(g-r)_0 = 0.0$ are young MS stars and that the BL feature and group of stars around (0.0, 21.0) are indeed helium-burning BL stars belonging to the same population. The 250 Myr isochrone seems to set a lower limit on the age, as its turnoff and BL seem to be too bright for the data. The 650 Myr isochrone shows that young stars also contribute to the RC, increasing the uncertainty in distance and age measurements using the RC luminosity, as these are age- and metallicity-dependent (Girardi & Salaris 2001). That the metallicity of the young stars is very difficult to determine is illustrated in Figure 2*d*, where 400 Myr isochrones with values of [Fe/H] of −2.3, −1.7, and −1.3 are overplotted. The regions of the CMD that are sensitive to the metallicity differences are too sparsely populated for this measurement to be made.

While the luminosity and color of the RC can be used to constrain population parameters such as distance, age, and metallicity, there are degeneracies, and solutions are generally not unique (Girardi & Salaris 2001). The presence of a RC, rather than a more extended HB, in itself implies that the stars are not both old and metal-poor ([Fe/H] < −2). However, since the metallicity of the older stars is relatively well constrained by the RGB slope, we can use the RC luminosity to determine either the distance or the age of the older stars, using the theoretical RC absolute *I*-band luminosities from Girardi & Salaris (2001). From our data, we determine the location of the RC by iteratively finding the mean color and magnitude of stars in a 0.25 mag × 0.5 mag box centered on the RC. Using different starting color and magnitude values around the approximate center, we find that $g_{0,\mathrm{RC}} = 23.71 \pm 0.03$ mag and $(g-r)_{0,\mathrm{RC}} = 0.43 \pm 0.02$ mag, where the errors are determined from bootstrap resampling tests. Using the photometric equations determined by R. Lupton,[8] this translates to $m_I = 22.76 \pm 0.04$ mag. The interplay between age and distance for the brightness of the RC, at a metallicity of [Fe/H] = −1.7, is illustrated in Figure 3, where we plot the absolute magnitude of RC stars as a function of age (Girardi & Salaris 2001). If we assume a distance modulus of 23.1 mag, the RC luminosity implies an average age for the older stars in Leo T of ∼7 Gyr. Alternatively, if we consider that the age of the stars might vary from 5 to 13 Gyr, as indicated by Figure 2*a*, this implies that the distance modulus lies between 22.9 and 23.2 mag.

[8] See http://www.sdss.org/dr5/algorithms/sdssUBVRITransform.html (R. Lupton 2005).

4. STRUCTURAL PROPERTIES

The stellar sources within 1.4′ from the center of Leo T are divided in two subsets corresponding to the young (<1 Gyr) and old (>5 Gyr) stellar populations described in § 3. This is done using the CMD selection boxes outlined in Figure 2*e*; by combining these two subsets, we create a third subset of both old and young Leo T candidate members. In this section we study the structural properties of these three subsets, which we will refer to as those containing "all," "young," and "old" stars, and which contain 2247, 854, and 1393 stars, respectively.

The central coordinates of Leo T were determined for the three subsets by iteratively calculating the mean center of the distribution of stars on the sky within an aperture of 6′ centered on the

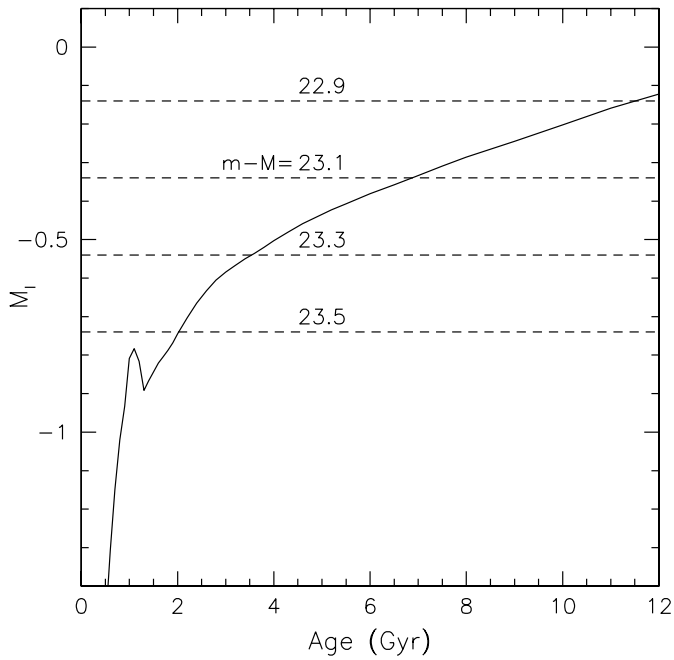

FIG. 3.—Relation between age and distance modulus determined from the RC luminosity. The solid line gives the absolute *I*-band magnitude of the RC stars as a function of age for a metallicity of [Fe/H] = −1.7, following Girardi & Salaris (2001). Dashed lines indicate the absolute magnitude of the RC in Leo T, assuming distance moduli of 22.9, 23.1, 23.3, and 23.5 mag from top to bottom. The intersection of each dashed line with the solid line gives the inferred age for each distance modulus.

TABLE 1
LEO T STRUCTURAL PROPERTIES

Parameter	All	Old	Young
R.A. (deg)	143.723 ± 0.001	143.727 ± 0.003	143.722 ± 0.001
R.A.	09 34 53.5 ± 0.2	09 34 54.5 ± 0.7	09 34 53.3 ± 0.2
Decl. (deg)	17.051 ± 0.001	17.050 ± 0.003	17.050 ± 0.001
Decl.	17 03 04 ± 4	17 03 00 ± 12	17 03 00 ± 4
r_e (arcmin)	0.59 ± 0.04	0.73 ± 0.08	0.51 ± 0.04
r_h (arcmin)	0.99 ± 0.06	1.22 ± 0.13	0.86 ± 0.07
r_c (arcmin)	0.68 ± 0.08	1.05 ± 0.27	0.54 ± 0.08
r_t (arcmin)	4.8 ± 1.0	4.5 ± 1.1	4.6 ± 1.1
r_e (pc)	72 ± 5	89 ± 10	62 ± 5
r_h (pc)	120 ± 7	148 ± 16	104 ± 8
r_c (pc)	82 ± 10	127 ± 33	65 ± 10
r_t (pc)	580 ± 120	550 ± 130	560 ± 130
c	7.1 ± 1.7	4.3 ± 1.5	8.6 ± 2.4
M_V (mag)	−8.0	−7.5	−6.9
$m-M_{\rm RC}$ (mag)	23.1 ± 0.2	...	...
$m-M_{\rm MATCH}$ (mag)	23.0 ± 0.2	...	...

NOTE.—Units of right ascension are hours, minutes, and seconds, and units of declination are degrees, arcminutes, and arcseconds.

assumed center, until the offset between subsequent iterations was zero. In Table 1, the right ascension and declination for each set of stars is listed. Errors in the obtained centers were determined using bootstrap resampling. There is a small offset of 0.3′, or 35 pc, between the centers of the distributions of the young and old stars, which is significant at the 2 σ level.

Figure 4 displays the surface density of stars as contour diagrams: Figures 4*a*, 4*b*, and 4*c* are for all stars, the old stars, and the young stars, respectively, and Figure 4*d* shows the contours of both the old and the young stars. The center of the distribution of all stars is indicated with a plus sign in Figures 4*a*–4*c* to help identify the apparent offset between the different subsets of stars. The contours correspond to densities of 1.5 σ, 3 σ, 6 σ, 12 σ, and 25 σ above the background, where σ is the Poisson uncertainty in the background stellar density. Leo T appears to be very compact and round, and there is little sign of any distortion or extratidal features. Fitting of a series of elliptical contours using the IRAF routine `ellipse` shows that for all subsets of stars, the ellipticity is below 0.1 out to a radius of 3′ from the center, where the density of stars drops below 1.5 σ above the background.

To measure the half-light radii, core radii, and limiting radii of Leo T and its subpopulations, King profiles and exponential profiles were fitted to the stellar distributions. For each subset of stars, the profiles were fitted to the stellar density in circular annuli of increasing radius and width, centered on the center found for that subset, as listed in Table 1. Crowding is not an issue for star counting down to the magnitude limit that we use (25.5 mag; see Fig. 2). The results for the exponential (r_e), half-light (r_h), core (r_c), and limiting (r_t) radii are listed in Table 1, and the density profiles with the corresponding best King profile fits are presented in Figure 5. The uncertainties on the fit parameters were determined using bootstrap resampling. Contrary to the tentative conclusion by Irwin et al. (2007) that the young stars seem to be less concentrated, comparing the density profiles from our deeper data shows unambiguously (∼3 σ) that the young stars are more centrally concentrated; their central density is 3 times higher than that of the old stars, whereas the limiting radii are indistinguishable. This leads to a difference of a factor of 2 in the concentration parameter $c = r_t/r_c$ between these populations.

To calculate the total *V*-band luminosity of Leo T, we convert the g_0 and r_0 magnitudes of all stars to *B* and *V*, using again the photometric transformations from R. Lupton.[9] The total luminosity in stars within a 5′ aperture centered on Leo T (5 times the half-light radius determined above), integrated between *V*-band magnitudes of 20.5 and 24.5 (∼1 mag below the RC), is $M_V = -7.1$ mag. This includes both old and young stars, but is not corrected for stars fainter than $V = 24.5$ mag and should therefore be taken as a minimum luminosity for Leo T. In this calculation a correction for the field stars has been done using the area outside a 6′ radius. Since the main-sequence turnoff of the young stars is at roughly $V = 24.5$ mag, most of the luminosity of the young population should be included in this estimate. For the older stars, we use the 10 Gyr, [Fe/H] = −1.5 luminosity function (LF) from Dotter et al. (2007), which assumes a Salpeter initial mass function (Salpeter 1955), and we find that the magnitude interval that we use should contain approximately 38% of the total light; for the young stars, we estimate that this should be ∼60% of the total light. Using the CMD box to select stars belonging to the older population, we get $M_{V,\rm old} = -6.4$ mag and $M_{V,\rm young} = -6.3$ mag, which are roughly equal values; including the LF correction yields $M_{V,\rm old} = -7.5$ mag and $M_{V,\rm young} = -6.9$ mag. Combining all this, we estimate the total luminosity of Leo T to be $M_{V,\rm total} \simeq -8.0$ mag. These fractions of the contributed light translate to a stellar mass fraction of the young stars of ∼10%, with some error, especially due to uncertainties in the initial mass function.

5. STAR FORMATION HISTORY

CMD-fitting techniques can be used to constrain the stellar population properties of dwarf galaxies in detail (e.g., Gallart et al. 1996; Tolstoy & Saha 1996; Aparicio et al. 1997; Dolphin 1997; Holtzman et al. 1999; Olsen 1999; Hernandez et al. 2000; Harris & Zaritsky 2001). Here we apply two different CMD-fitting packages, StarFISH (Harris & Zaritsky 2001) and MATCH (Dolphin 2002), to our photometry of stars within 1.4′ of the center of Leo T and use the results to constrain its star formation history and metallicity evolution.

Both CMD-fitting packages are based on the same principles, although the exact implementation differs slightly. On the basis

[9] See http://www.sdss.org/dr5/algorithms/sdssUBVRITransform.html (R. Lupton 2005).

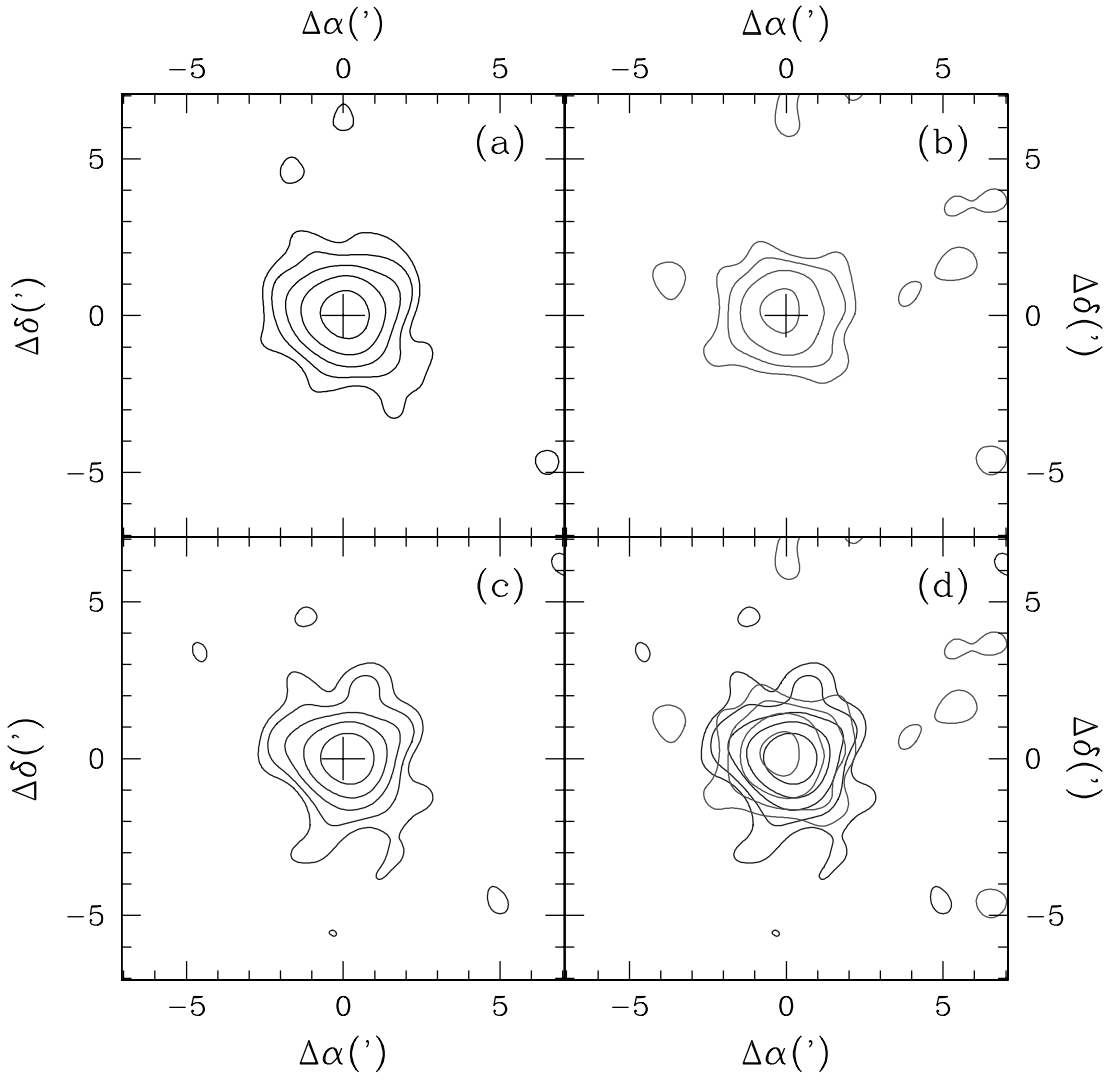

FIG. 4.—Stellar density distributions in Leo T for (*a*) all stars, (*b*) the old stars, (*c*) the young stars, and (*d*) both the old (*medium gray contours*) and the young (*dark gray contours*) stars. These density maps are smoothed with a 0.6′ Gaussian smoothing kernel, and the contours correspond to densities of 1.5 σ, 3 σ, 6 σ, 12 σ, and 25 σ above the background. As a reference, the plus sign in panels *a*–*c* indicates the center of the distribution of all stars. [*See the electronic edition of the Journal for a color version of this figure.*]

of theoretical isochrones, where here we use those from Girardi et al. (2004), artificial CMDs are constructed for different combinations of stellar population parameters such as distance, age, metallicity, initial mass function, and binary fraction. Convolving these theoretical CMDs with the photometry errors and completenesses determined from the artificial star tests yields realistic model CMDs that can be compared to the data. Converting the models and data to Hess diagrams enables a direct pixel-to-pixel comparison. The fit result is the best-fitting linear combination of model CMDs, where the scaling of each model is the star formation rate (SFR) for the corresponding stellar population bin. To correct for contamination by foreground stars, a control CMD can be provided, which is then used as an additional model CMD in the fit. Here we use the stars outside a 6′ radius from the center of Leo T for the control CMD.

For the star formation history (SFH) fits with MATCH, we chose a set of metallicity bins centered at values of [Fe/H] of −2.2, −1.7, −1.3, and −0.8 dex, each with a width of 0.5 dex. Two sets of age bins were adopted, one with bin widths of $\Delta \log(t) = 0.3$ dex and one with bin widths of $\Delta \log(t) = 0.4$ dex, running from ∼10 Myr to ∼16 Gyr. Stars with colors in the range $-1.0 \text{ mag} < (g-r)_0 < 2.0$ mag and that were brighter than $g_0 = 26$ mag and $r_0 = 25$ mag were fitted, using a Hess diagram bin size of 0.15 in magnitude and 0.08 in color.

With the foreground extinction having been corrected on the basis of the dust extinction maps of Schlegel et al. (1998) and the age and metallicity having been fitted by the software, the remaining parameter is the distance to Leo T. In order to constrain this parameter and to determine how sensitive the best-fitting SFHs are to the adopted distance, fits were run for a range of distance moduli between 22.6 and 23.6 mag, at intervals of 0.05 mag. Figure 6 shows the fit qualities for these fits, normalized by that of the best fit. The two different age-binning schemes give slightly different best distances. The overall best fit is obtained with the smaller age bins, which is to be expected, since that binning scheme provides more age bins and thus has more degrees of freedom. If we take the expected variance in the fit quality into account, the statistically "good" fits can be determined. These fits have distance moduli that range from 22.8 to 23.2 mag, thus giving a distance estimate of $m - M = 23.0 \pm 0.2$ mag. On the basis of the RC luminosity calculated in § 3, a distance modulus of 23.0 mag implies an average age for the stars in Leo T of ∼9 Gyr (Fig. 3). Using the fits with distance moduli between 22.8 and 23.2 mag, the SFH and metallicity evolution were determined.

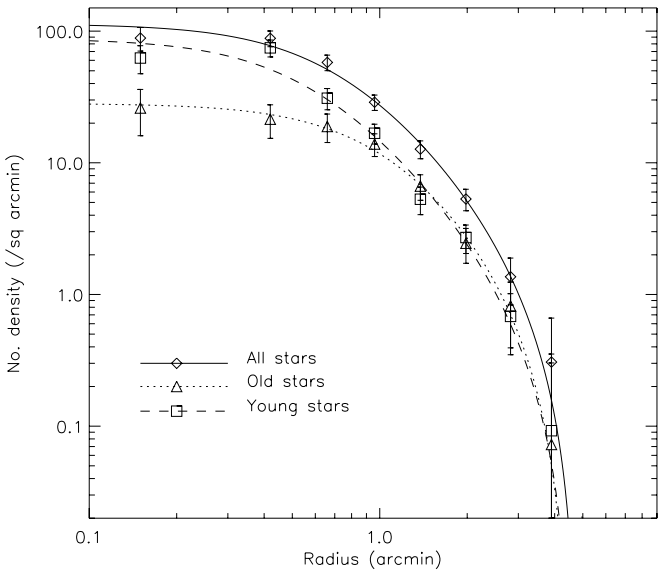

FIG. 5.—Background-corrected radial profiles of Leo T, determined from the CMD-selected subsets for young (*squares*), old (*triangles*), and all (*diamonds*) stars. The lines represent the best-fitting King profiles, determined for each subset of stars separately: the dashed line for the young stars, the dotted line for the old stars, and the solid line for all stars.

In Figure 7 the relative star formation rate and the metallicity are plotted as a function of time.

For the StarFISH fit, we matched the input parameters as closely as possible to those used in the MATCH analysis. We adopted a distance modulus of 23.0 mag and used the extinction values from the Schlegel et al. (1998) map. We also used two sets of age bins, with $\Delta\log(t) = 0.3$ and 0.4 dex, and one metallicity bin, centered at $[\mathrm{Fe/H}] = -1.5$, based on the metallicity estimates from the MATCH fit. StarFISH was allowed to fit stars from -1 to 3 mag in $(g - r)_0$, from 17 to 26 mag in g_0, and from 17 to 25 mag in r_0, with a bin size of 0.15 mag in each dimension.

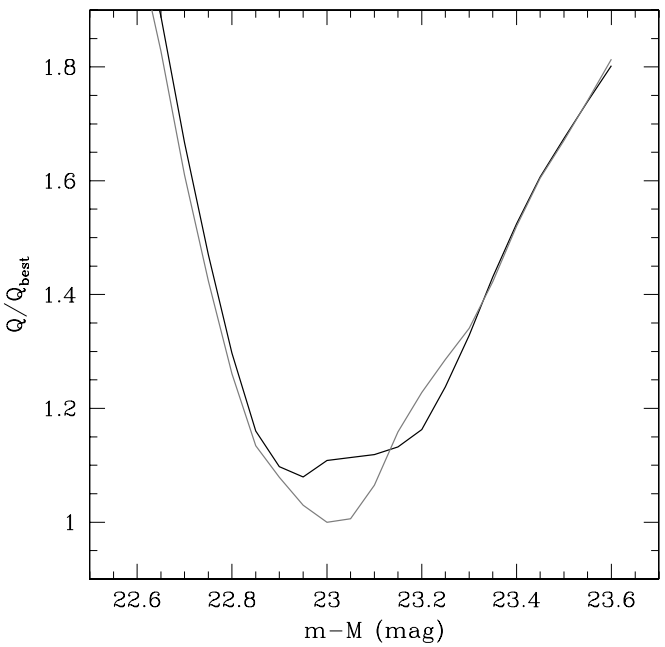

FIG. 6.—Goodness of fit relative to that of the best fit for MATCH SFH fits, assuming different distance moduli. The gray line is for age bins of width $\Delta\log(t) = 0.3$ width, and the black line is for age bins of width $\Delta\log(t) = 0.4$.

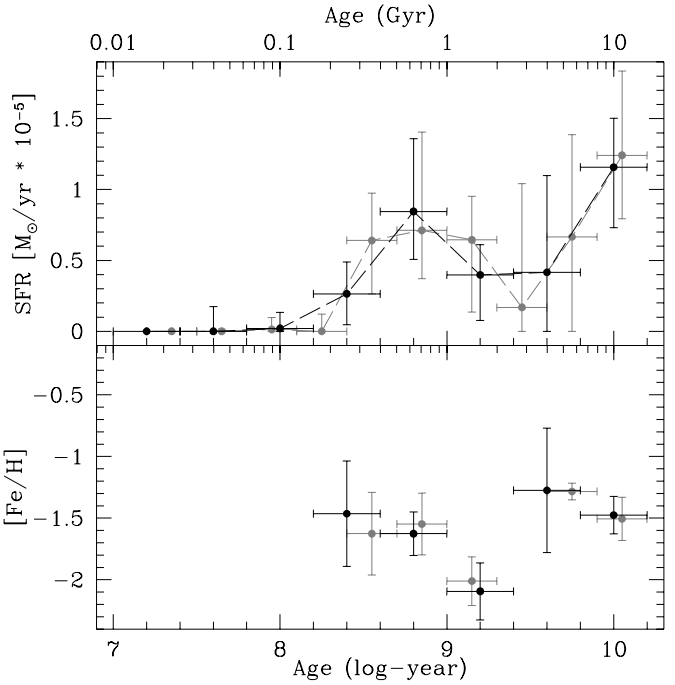

FIG. 7.—Star formation rate and metallicity evolution of Leo T from fits with MATCH. *Top*: Star formation as a function of time for age bins of widths $\Delta\log(t) = 0.3$ (*gray circles*) and $\Delta\log(t) = 0.4$ (*black circles*). Horizontal error bars indicate the bin width. *Bottom*: Metallicity as a function of time, with symbols and horizontal error bars as above. The metallicities are the SFR-weighted average.

The best-fit StarFISH solutions for the two age-binning schemes are shown in Figure 8.

Figure 9 shows a comparison of the best-fit models to the data. The MATCH and StarFISH results are in statistical agreement: in both cases, we find extended star formation spanning ages from a

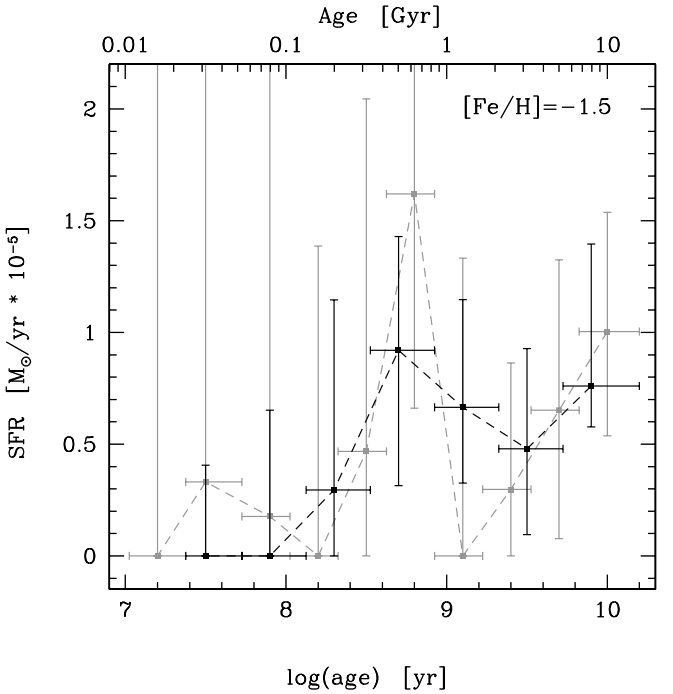

FIG. 8.—SFH solution from the StarFISH fit. Here the SFH is expressed as the SFR(t) for a metallicity of $[\mathrm{Fe/H}] = -1.5$. As in Fig. 7, the solution with $\Delta\log(t) = 0.4$ is shown in black, and the solution with $\Delta\log(t) = 0.3$ is shown in gray.

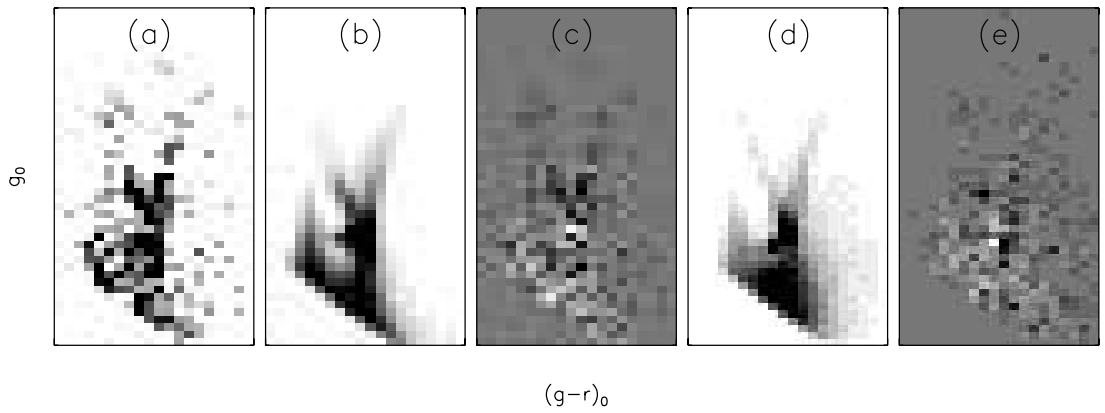

FIG. 9.—Comparison of data to best MATCH and StarFISH model fits. (*a*) A $(g - r)_0$ vs. g_0 Hess diagram of the stars within 1.4′ of the Leo T center (i.e., the population used in the SFH analysis). (*b*) The Hess diagram of the synthetic population corresponding to the best-fit MATCH solution. (*c*) The residual Hess diagram after subtracting the best-fit MATCH model from the data. (*d*) Hess diagram of the synthetic population corresponding to the best-fit StarFISH solution. (*e*) The residual Hess diagram after subtracting the best-fit StarFISH model from the data. The sharp cutoff at faint magnitudes is caused by the limiting magnitudes of $g_0 = 26$ mag and $r_0 = 25$ mag used with the fits.

few hundred Myr to 12 Gyr. The MATCH solution finds the metallicity to be roughly [Fe/H] $= -1.5$ and indicates two distinct epochs of star formation, one at 6–12 Gyr and one at 0.4–1 Gyr. This bimodality is also present in the higher resolution StarFISH solution. These results are also in agreement with the SFH for Leo T derived by de Jong et al. (2008), which was based on much shallower SDSS data. The star formation rates in the two distinct episodes in the higher resolution fits confirm that the young stellar population represents approximately 10% of the stellar mass in Leo T.

The difference in the error bars on the star formation rates between Figures 7 and 8 is due to the different ways in which they are determined. In the case of MATCH, error bars are determined in two ways. First, for each age bin the minimum and maximum star formation rates are found in the set of models that qualify as "good fits." If all "good fit" models give the same star formation rate in a particular age bin, this error component for that particular bin would be zero. Second, Monte Carlo simulations are done to assess the uncertainty associated with the sparseness of the sampling of the CMD. For this, CMDs are drawn from the best-fit CMD model and their SFHs are determined. The scatter in the star formation rates and metallicities for each age bin is the second error component. These two error components are added quadratically to give the final error bars. StarFISH, on the other hand, determines error bars by measuring the confidence intervals of each amplitude through a systematic exploration of parameter space in the vicinity of the best fit. First, each amplitude is varied in turn while holding all others at their best-fit values. This determines the independent uncertainty on each amplitude. Next, amplitude pairs that are similar in age or metallicity are varied together while holding all other amplitudes at their best-fit values. This determines the covariant uncertainties between amplitude pairs that may be partially degenerate. Finally, the parameter space is explored uniformly by deviating from the best-fit location along a series of random "directions" in parameter space. We step along each direction until the fitting statistic increases to our "good fit" limit. The random-direction search is performed many thousands of times. The final error bars are the maximum and minimum value of each amplitude for all tested parameter-space locations whose fitting statistics fell under the "good fit" threshold. This difference in approach leads to very different error bars at the young end, where the StarFISH error bars (Fig. 8) are very large because the upper main sequence is very poorly populated and thus is poorly constrained. On the other hand, this lack of evidence for very young (<100 Myr) stars causes the MATCH error bars in these bins to be very small (Fig. 7). However, on the basis of these data, some low-level ongoing star formation cannot be strictly excluded.

Since the data do not reach the ancient main-sequence turnoff at the distance of Leo T, the SFH solutions for ages older than a few Gyr are based entirely on the morphology of the red giant and horizontal branches. In particular, at metallicities around [Fe/H] $= -1.5$, truly ancient core helium-burning stars are predicted to extend slightly blueward of the canonical "red clump" feature (see the 12.5 Gyr isochrone plotted in Fig. 2*a*). The subtlety of this feature in the CMD contributes to the uncertainty of the derived star formation rate in the oldest age bin.

6. SUMMARY AND CONCLUSIONS

On the basis of deep g_0 and r_0 photometry obtained with the LBT, we have studied the stellar populations and structural properties of the Leo T dwarf galaxy. A comparison of the background-subtracted Hess diagram with theoretical isochrones confirms the presence of very young stars with ages between ~200 Myr and 1 Gyr, as well as an older stellar population (>5 Gyr), the latter with a likely metallicity of [Fe/H] $\simeq -1.7$. The stellar mass in the young population is estimated to be ~10% of the total stellar mass. On the basis of the apparent magnitude of the RC stars, we determine the distance modulus of Leo T to be 23.1 ± 0.2 mag, confirming the value from Irwin et al. (2007). The total luminosity of Leo T is estimated to be $M_{V,\mathrm{total}} \simeq -8.0$ mag, almost 1 mag higher than the estimate from the discovery paper. If we use the mass estimate for Leo T from Simon & Geha (2007), this implies a mass-to-light ratio of ~60 $M_\odot/L_{V,\odot}$.

A more sophisticated analysis of the photometry using CMD-fitting techniques yields similar results. The distance determination gives a distance modulus of $m - M = 23.0 \pm 0.2$ mag. CMD fits with two different software packages both indicate two distinct episodes of star formation, one at ~6–12 Gyr and one at ~0.4–1 Gyr, although the drop in the star formation rate in between has a low significance. From the CMD fits, no strong metallicity evolution is apparent, with an approximate metallicity of [Fe/H] ~ −1.5 at all times. The metallicity seems to have a small dip around $\log(t) = 9.2$, but since the metallicity constraints at that age come from regions of the CMD where the stellar models are least reliable, such as the RC and the asymptotic giant branch, this is not significant.

Old and young stars were preferentially selected using CMD selection boxes in order to study their individual spatial distributions. The young stars are more strongly concentrated near the center of Leo T, but both components display the same spatial extent. There seems to be a slight offset between the young and old stars, but from these data this is hardly significant. Since stars are formed in clusters, young stars are usually spatially more strongly confined than older stars. This has also been found in other dwarf galaxies (e.g., Hurley-Keller et al. 1999; Martínez-Delgado et al. 1999; Harbeck et al. 2001; Battaglia et al. 2006; McConnachie et al. 2006; Martin et al. 2008). The half-light radius for all stars is found to be 120 ± 7 pc, which is slightly smaller than the value from Irwin et al. (2007).

Comparing our results with the properties of the other transition-type dwarf galaxies in the Local Group, DDO 210, Phoenix, Pisces, Antlia, Pegasus, and Leo A (e.g., Mateo 1998; Grebel 2001), shows a lot of similarities. The presence of both stars of old or intermediate (>5 Gyr) ages and very young (<1 Gyr) stars is common, as is the metallicity of $[\mathrm{Fe/H}] \sim -1.5$. A similar apparent lack of metallicity evolution was found in Leo A by Cole et al. (2007). Although Leo T is similar to most other transition galaxies in terms of total mass and H I mass, it is much fainter. Our luminosity estimate of $M_{V,\mathrm{total}} \simeq -8.0$ is 2 mag fainter than that for any of the other transition objects (e.g., Mateo 1998). Therefore, Leo T remains the least luminous galaxy with recent star formation known.

We find no evidence for tidal distortion of Leo T. This is not unexpected, since it is at a large distance from the Milky Way and M31, although, on the basis of the limited information about its orbit, the possibility cannot be excluded that Leo T has come close to the Milky Way at some time in the past. However, the lack of distortion implies that its low mass and luminosity are intrinsic, rather than being the result of interaction or disruption. Thus, the case of Leo T suggests that isolated halos with masses of as low as $10^7 M_{\odot}$ are able to accrete and/or retain gas and form stars for at least a Hubble time.

The authors thank the LBT Science Demonstration Time (SDT) team for assembling and executing the SDT program and thank the LBC team and the LBTO staff for their kind assistance. We also thank Chris Kochanek for help with preparing the manuscript and the anonymous referee for useful comments and advice.

REFERENCES

Adelman-McCarthy, J. K., et al. 2007, ApJS, 172, 634
Aparicio, A., Gallart, C., & Bertelli, G. 1997, AJ, 114, 680
Battaglia, G., et al. 2006, A&A, 459, 423
Belokurov, V., et al. 2006, ApJ, 647, L111
———. 2007, ApJ, 654, 897
Cole, A. A., et al. 2007, ApJ, 659, L17
Coleman, M. G., et al. 2007, ApJ, 668, L43
de Jong, J. T. A., Rix, H.-W., Martin, N. F., Zucker, D. B., Dolphin, A. E., Bell, E. F., Belokurov, V., & Evans, N. W. 2008, AJ, 135, 1361
Dolphin, A. E. 1997, NewA, 2, 397
———. 2002, MNRAS, 332, 91
Dotter, A, Chaboyer, B., Jevremović, D., Baron, E., Ferguson, J. W., Sarajedini, A., & Anderson, J. 2007, AJ, 134, 376
Gallart, C., Aparicio, A., Bertelli, G., & Chiosi, C. 1996, AJ, 112, 1950
Giallongo, E., et al. 2008, A&A, 482, 349
Girardi, L., Grebel, E. K., Odenkirchen, M., & Chiosi, C. 2004, A&A, 422, 205
Girardi, L., & Salaris, M. 2001, MNRAS, 323, 109
Grebel, E. K. 2001, Ap&SS Suppl., 277, 231
Harbeck, D., et al. 2001, AJ, 122, 3092
Harris, J., & Zaritsky, D. 2001, ApJS, 136, 25
Hernandez, X., Gilmore, G., & Valls-Gabaud, D. 2000, MNRAS, 317, 831
Hess, R. 1924, in Probleme der Astronomie: Festschrift für Hugo V. Seeliger, ed. H. Kienle (Berlin: Springer), 265
Hill, J. M., Green, R. F., & Slagle, J. H. 2006, Proc. SPIE, 6267, 62670Y
Holtzman, J. A., et al. 1999, AJ, 118, 2262
Hurley-Keller, D., Mateo, M., & Grebel, E. K. 1999, ApJ, 523, L25
Irwin, M. J., et al. 2007, ApJ, 656, L13
Martin, N. F., et al. 2008, ApJ, 672, L13
Martínez-Delgado, D., Gallart, C., & Aparicio, A. 1999, AJ, 118, 862
Mateo, M. L. 1998, ARA&A, 36, 435
McConnachie, A. W., Arimoto, N., Irwin, M., & Tolstoy, E. 2006, MNRAS, 373, 715
Olsen, K. A. G. 1999, AJ, 117, 2244
Ragazzoni, R., et al. 2006, Proc. SPIE, 6267, 626710
Ryan-Weber, E. V., Begum, A., Oosterloo, T., Pal, S., Irwin, M. J., Belokurov, V., Evans, N. W., & Zucker, D. B. 2008, MNRAS, 384, 535
Salpeter, E. E. 1955, ApJ, 121, 161
Schlegel, D., Finkbeiner, D., & Davis, M. 1998, ApJ, 500, 525
Simon, J. D., & Geha, M. 2007, ApJ, 670, 313
Tolstoy, E., & Saha, A. 1996, ApJ, 462, 672
Walsh, S. M., Jerjen, H., & Willman, B. 2007, ApJ, 662, L83
Willman, B., et al. 2005a, AJ, 129, 2692
———. 2005b, ApJ, 626, L85
York, D. G., et al. 2000, AJ, 120, 1579
Zucker, D., et al. 2006a, ApJ, 643, L103
———. 2006b, ApJ, 650, L41